Mn Modified Ni/Bentonite for CO$_2$ Methanation

Yuexiu Jiang [1], Tongxia Huang [1], Lihui Dong [1], Tongming Su [1], Bin Li [1], Xuan Luo [1], Xinling Xie [1,*], Zuzeng Qin [1,2,*] , Cuixia Xu [3] and Hongbing Ji [1,2]

[1] School of Chemistry and Chemical Engineering, Guangxi Key Laboratory of Electrochemical Energy Materials, Guangxi University, Nanning 530004, China; jiangyuexiu@126.com (Y.J.); htx@bipt.edu.cn (T.H.); donglihui2005@126.com (L.D.); sutm@gxu.edu.cn (T.S.); binli@gxu.edu.cn (B.L.); luo.lqlf@163.com (X.L.); jihb@sysu.edu.cn (H.J.)

[2] School of Chemistry, Sun Yat-sen University, Guangzhou 510275, China

[3] Dan F. Smith Department of Chemical Engineering, Lamar University, Beaumont, TX 77710, USA; cxu@lamar.edu

* Correspondence: xiexinling@126.com (X.X.); qinzuzeng@gxu.edu.cn (Z.Q.);
   Tel.: +86-771-3233718 (X.X.); +86-771-3273701 (Z.Q)

Abstract: To enhance the low-temperature catalytic activity and stability of Ni/bentonite catalyst, Ni-Mn/bentonite catalyst was prepared by introducing Mn into Ni/bentonite catalyst and was used for CO$_2$ methanation. The results indicated that the addition of Mn enhanced the interaction between the NiO and the bentonite carrier, increased the dispersion of the active component Ni and decreased the grain size of the active component Ni, increased the specific surface area and pore volume of the Ni/bentonite catalyst, and decreased the average pore size, which suppressed the aggregation of Ni particles grown during the CO$_2$ methanation process. At the same time, the Mn addition increased the amount of oxygen vacancies on the Ni/bentonite catalyst surface, which promoted the activation of CO$_2$ in the methanation reaction, increasing the low-temperature activity and stability of the Ni/bentonite catalyst. Under the reaction condition of atmospheric pressure, 270 °C, V(H$_2$):V(CO$_2$) = 4, and feed gas space velocity of 3600 mL·g$_{cat}$$^{-1}$·h^{-1}, the CO$_2$ conversion on the Ni-Mn/bentonite catalyst with 2wt% Mn was 85.2%, and the selectivity of CH$_4$ was 99.8%. On the other hand, when Mn was not added, the CO$_2$ conversion reached 84.7% and the reaction temperature only raised to 300 °C. During a 150-h stability test, the CO$_2$ conversion of Ni-2wt%Mn/bentonite catalyst decreased by 2.2%, while the CO$_2$ conversion of the Ni/bentonite catalyst decreased by 6.4%.

Keywords: CO$_2$ methanation; Ni/bentonite catalyst; Solution combustion synthesis; Mn modification

1. Introduction

With the development of modern society and the increasing combustion of fossil fuels, the CO$_2$ concentration in the atmosphere has increased in recent years, causing global warming and even climate change [1,2]. Hence, CO$_2$ capture and sequestration (CCS) and conversion continue to play a key role in reducing the atmospheric CO$_2$ concentration and make the transition towards green energy smoother, especially in carbon-intensive regions [3–6].

Catalytic hydrogenation of CO$_2$ to methane, also called the Sabatier reaction, is an important reaction in CO$_2$ utilization [7,8]; it is also a simple and environment-friendly process, and the main product, methane (CH$_4$), is the main constituent of natural gas, which has the advantages of high calorific value and environmental protection. CH$_4$ demands have been increasing in recent years [9,10]. At present, Rh/γ-Al$_2$O$_3$ [11,12], Ni/Al$_2$O$_3$ [13,14], Ni/ZrO$_2$ [15–17], Ni/CeO$_2$ [17–19], Ni/USY zeolites [20,21], and Ni/La$_2$O$_3$ [17,22] have been used for the catalytic hydrogenation of CO$_2$ to CH$_4$. Among them, the Ni-based catalysts have been widely used in CO$_2$ hydrogenation due to

their lower cost than the noble metal-based catalysts, high catalytic properties and they are easily obtainable [10,13,14,22]. CO_2 is an inert molecule which is difficult to be activated at low temperature; therefore, higher CO_2 conversion can only be obtained at higher temperatures above 350 °C, leading to an adverse influence on the catalysts stability/lifetime, easy to sinter deactivation [23], and increased energy consumption [24]. Therefore, to reduce the reaction temperature, low-temperature activity Ni-based catalysts should be developed.

In our previous study [25], Ni/bentonite with higher catalytic CO_2 methanation activity was prepared by using a solution combustion synthesis (SCS), which has the advantage of simple prepared apparatus, rapid reaction rates, low-cost, and relatively low preheating temperatures [26]; furthermore, the fuel in SCS provided energy in the combustion and was used as a complexing agent to form a complex with metal ions, which increase its solubility. However, the lower temperature activity and stability of the Ni/bentonite catalysts prepared by SCS were still low [25].

In general, the addition of a small amount of rare earth or transition metal could effectively reduce the catalytic hydrogenation reaction temperature, i.e., Ni^{2+} could be partially substituted with Co^{3+} ions to form a Ni-Co spinel solid solution, and is vital for CO oxidation [27]; Fe modified Mn/TiO_2 catalysts showed distinguished catalytic activities in the NH_3-SCR reaction [28]; the addition of La and Mn additives facilitated the dispersion of Ni species, and increased the syngas methanation activities of Ni catalysts [29]. Among them, transition metal Mn exhibited the properties of the adjusted d-electron structure and could improve the surface area of the active metal, as well as the metal dispersion on the support [30]. In the present study, to improve the catalytic activities and stabilities of the Ni/bentonite catalysts, based on the previous research about the Ni-based catalysts [25,31,32], Mn was used to modify the Ni/bentonite prepared by SCS using urea as a fuel, and was applied in the CO_2 catalytic hydrogenation to CH_4. Furthermore, the Ni/bentonite catalysts were characterized by X-ray diffraction (XRD), H_2 temperature-programmed reduction (H_2-TPR), scanning electron microscope (SEM), N_2-adsorption/desorption, and X-ray photoelectron spectroscopy (XPS).

2. Results and Discussion

2.1. Effects of Metal Modification on CO_2 Methanation on Ni/Bentonite

The addition of a small amount of other metal elements to the Ni catalyst has an effect on the catalytic activity. The addition of 2 wt% Na, Mg, or Mn respectively influenced the catalytic activity. The Ni/ bentonite-U (U means the Urea was used as the fuel in a SCS) catalysts were modified by adding 2 wt% Na, Mg, Mn, Ce, and La, respectively, and were used in the methanation of CO_2. The activities of the catalysts before and after the modification were compared and the results are shown in Figure 1.

From Figure 1, at 200–350 °C, the activity order of the CO_2 conversion in the CO_2 methanation for the Ni/bentonite-U catalysts was: Ni-Mn/bentonite-U > Ni-Ce/bentonite-U > Ni-La/bentonite-U > Ni-Mg/bentonite-U ≈ Ni/bentonite-U > Ni-Na/bentonite-U. Considering the order, the CO_2 conversion on the Ni/bentonite-U catalyst was reduced after adding Na. The reduction might be attributed to the fact that the addition of Na covered some of the Ni active sites and weakened the adsorption ability of the reactant molecules on the surface of Ni/bentonite catalysts [33]. In Figure 1, the addition of Mg did not exhibit a significant effect on CO_2 conversion in the CO_2 methanation, which may be due to the formation of the stronger interaction between Ni and Mg oxides, leading to the decreased amount of nickel-active sites available and thus the catalytic performance [34]. However, the addition of La, Ce and Mn increased the CO_2 conversion of Ni/bentonite-U catalysts at low temperature, which might be due to the fact that the addition of these three metals could promote the structure and performance of the catalysts, form oxygen vacancies, change the interaction between the active component Ni and the support, and the CO_2 could be activated by the basic sites formed between the metal and the Ni, which further improved the catalytic activity of the catalysts [35–40]. Among these five metals, the addition of Mn had the most significant improvement with regards to

catalyst activity. Therefore, the influence of the additive on the catalytic activity and stability of the catalysts was investigated by selecting the Mn promoter.
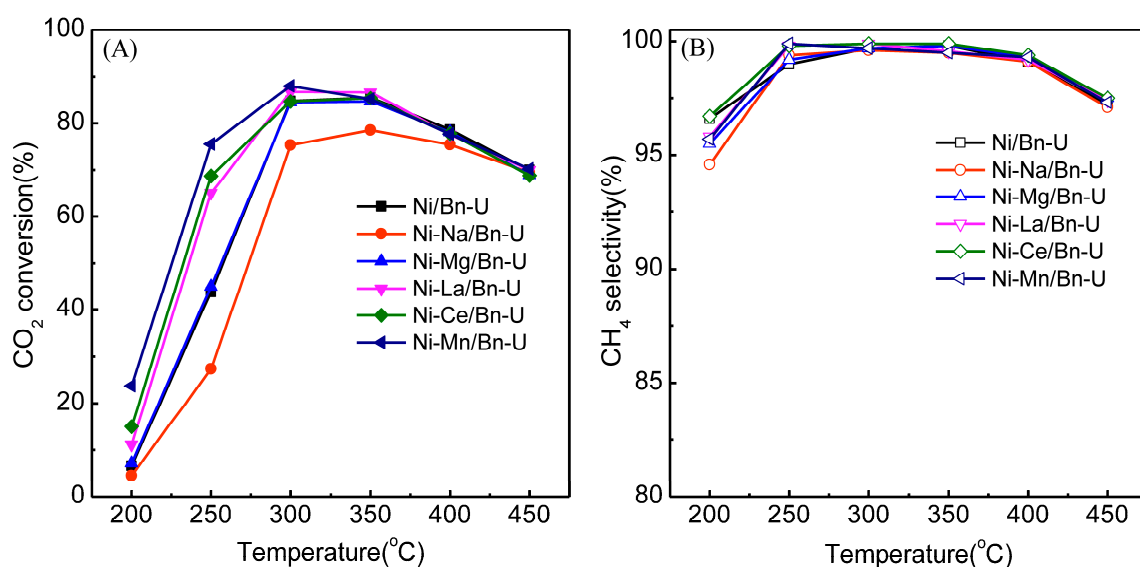

Figure 1. Effects of Ni/bentonite-U catalyst modified with different metals on the CO_2 conversion (**A**) and CH_4 selectivity (**B**). Reaction conditions: atmospheric pressure, $V(H_2)/V(CO_2) = 4$, GHSV = 3600 mL·g_{cat}^{-1}·h^{-1}.

2.2. The Effects of the Mn on the CO_2 Methanation on Ni/bentonite Catalysts

The Ni-Mn/bentonite-U catalysts with the Mn contents of 0, 1.0, 2.0, and 3.0 wt% were prepared by the impregnation combustion method, and the catalysts were used in CO_2 methanation. Figure 2 shows the effects of the Mn contents on the catalytic activity of the Ni-Mn/bentonite-U catalysts.
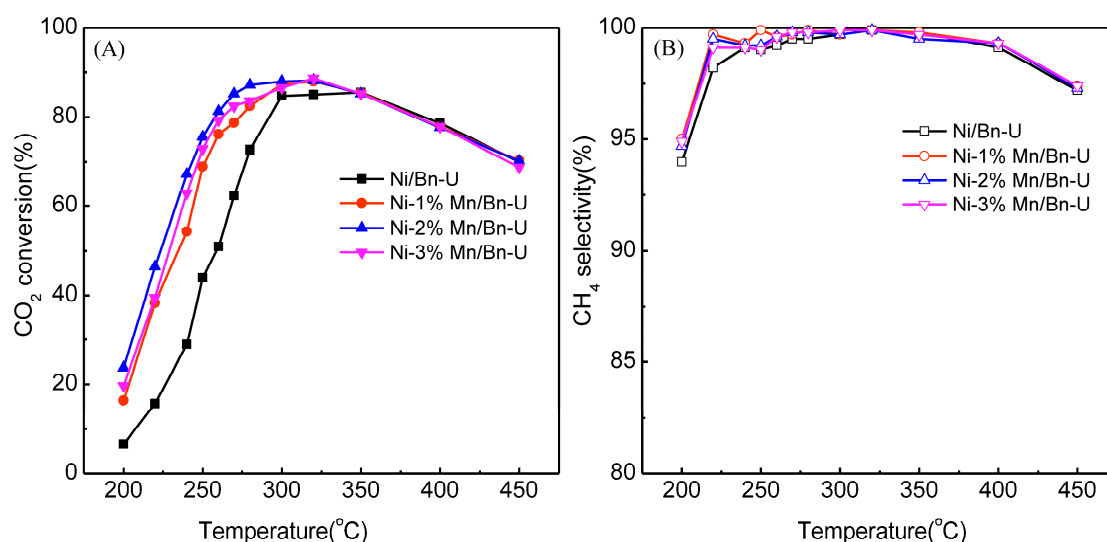

Figure 2. Effects of Ni/bentonite-U catalyst with different Mn amounts on the CO_2 conversion (**A**) and CH_4 selectivity (**B**). Reaction conditions: atmospheric pressure, $V(H_2)/V(CO_2) = 4$, *GHSV* = 3600 mL·g_{cat}^{-1}·h^{-1}.

The CO_2 conversion on the Ni-Mn/bentonite-U and the Ni/bentonite-U catalysts increased with increasing temperature from 200 to 300 °C. The CO_2 conversion on the Ni-Mn/bentonite-U catalyst was higher than that on the Ni/bentonite-U catalysts in 200–300 °C. The CO_2 conversion on the Ni-Mn/bentonite-U and the Ni/bentonite-U catalysts decreased gradually above 300 °C.

The highest CO_2 conversion 88.0% was obtained when the content of Mn reached 2wt% and the CH_4 selectivity was approximately 99.7% at 300 °C on the Ni-2wt%Mn/bentonite-U catalyst. In the same conditions, the CO_2 conversion and CH_4 selectivity were 84.7% and 99.7% at 300 °C, respectively, on the Ni/bentonite-U. Therefore, The Mn could increase the CO_2 conversion at low temperature, and 2wt% Mn was chosen as the optimal addition amount to investigate the effects of the Mn on the structure and surface properties of the Ni/bentonite-U catalysts.

2.3. XRD Analysis

Figure 3 shows the XRD patterns of the Ni/bentonite-U and the Ni-2wt%Mn/Bentonite-U catalysts after 4 h calcining at 400 °C. Four diffraction peaks (2θ = 19.8°, 34.9°, 54.2°, and 62.0°), which were the characteristic diffraction peaks of montmorillonite, were both found in the spectra of the Ni/bentonite-U and the Ni-2wt%Mn/bentonite-U catalysts, indicating that montmorillonite was the main component in bentonite. The diffraction peaks (2θ = 37.2°, 43.3°, 62.9°, 75.4°, and 79.4°) of NiO (JCPDS card NO. 47-1049) were both detected in the Ni/bentonite-U and the Ni-2wt%Mn/bentonite-U catalysts, which ascribed to the planes (111), (200), (220), (311), and (222) of the NiO cubic phase, respectively. No diffraction peaks of the Mn were found in the XRD patterns of the Ni-Mn/bentonite-U samples, which might be due to the low Mn content, the amorphous state of Mn, or the highly dispersion of Mn on the catalyst surface [27].
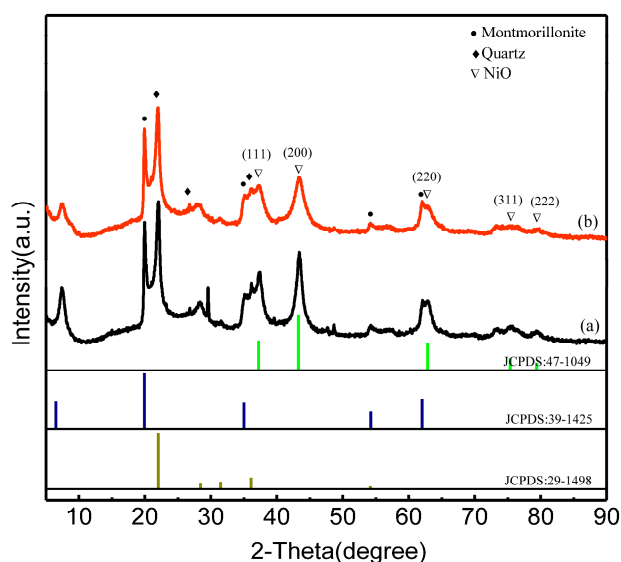

Figure 3. XRD patterns of the Ni/Bentonite-U (a) and Ni-2wt%Mn/Bentonite-U (b) after being calcined at 400 °C.

In addition, the intensity of NiO diffraction peaks in the Ni-2wt%Mn/bentonite-U catalyst was remarkably weaker than the intensity of NiO diffraction peaks in the Ni/bentonite-U catalyst. According to the diffraction plane (200), the average grain sizes of NiO in different catalysts were calculated by the Scherrer's equation. NiO had a smaller grain size in Ni-2wt%Mn/bentonite-U catalyst (5.3 nm) than in the Ni/bentonite-U catalyst (8.2 nm), which demonstrated that the addition of Mn decreased the average grain sizes of NiO and promoted NiO dispersion on bentonite [41]. The smaller Ni particles could promote the activation of CO_2 by promoting H spillover to the surface of the carrier and enhancing the CO_2 methanation activity [42].

2.4. SEM Analysis

Figure 4 showed the SEM images of the Ni/bentonite-U and Ni-2wt%Mn/bentonite-U catalysts after the reduction, and the effects of Mn on the morphologies and the catalyst structures were investigated.
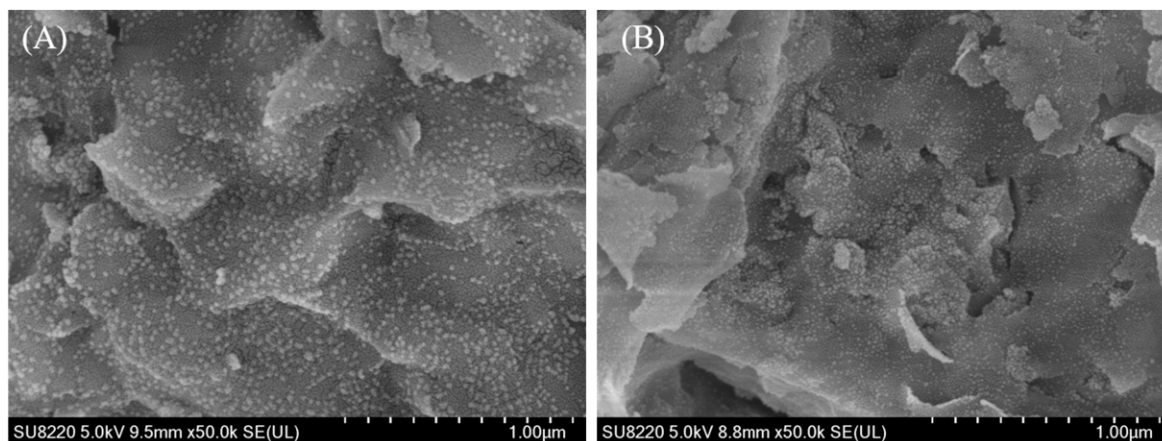
Figure 4. SEM images of the reduced Ni/bentonite-U (**A**) and Ni-2wt%Mn/bentonite-U (**B**) catalysts.

As shown in Figure 4A,B, the Ni/bentonite-U and the Ni-2wt%Mn/bentonite-U catalysts were irregularly spherical, indicating that adding Mn did not change the morphologies of the Ni/bentonite-U catalyst. After adding Mn, the Ni particles were uniformly dispersed on the surface of the reduced Ni-2wt%Mn/bentonite-U catalyst and the Ni particle size was about 15 nm, which was smaller than the particle size of Ni in the Ni/bentonite-U catalysts (20 nm). It was concluded that adding Mn prohibits the aggregation of Ni particles, resulting in a decrease of Ni particle size [43,44].

2.5. N_2 Adsorption-Desorption Analysis

The N_2 adsorption–desorption and pore size distribution of the Ni/bentonite-U and the Ni-2wt%Mn/bentonite-U catalysts are shown in Figure 5, and the specific surface area and average pore size calculated by BET and BJH methods are summarized in Table 1.
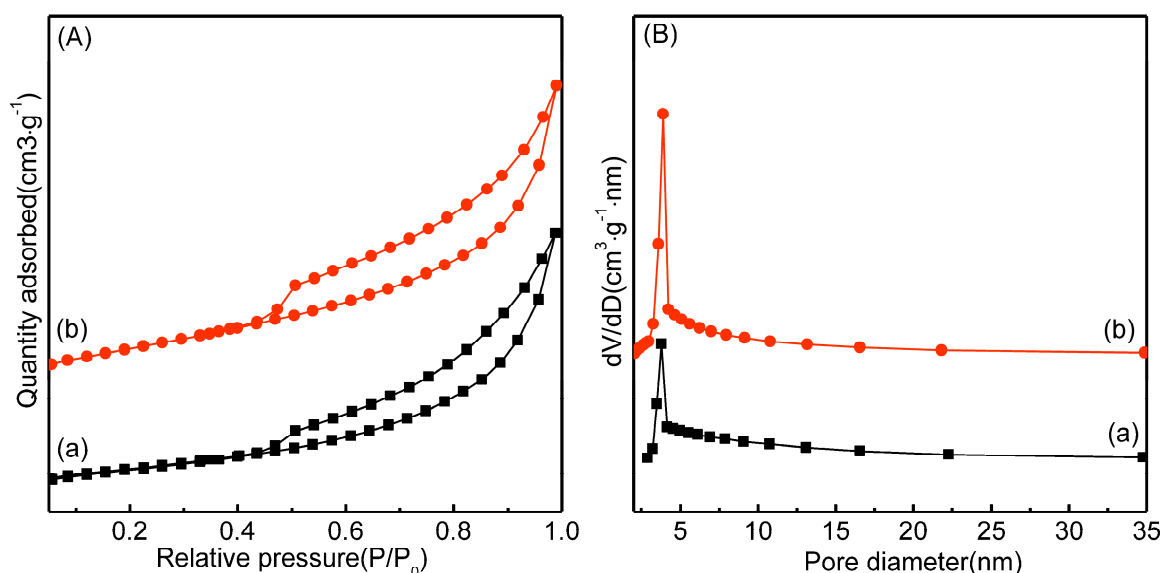

Figure 5. N_2 adsorption-desorption isotherms (**A**) and pore diameter distributions profiles (**B**) of Ni/Bentonite-U (a) and Ni-2wt%Mn/Bentonite-U (b).

According to the IUPAC classification, the N_2 adsorption–desorption isotherm of the Ni/bentonite-U and the Ni-2wt%Mn/bentonite-U catalysts can be attributabled to the IV-type isotherm, as shown in Figure 5A. In the medium- and high-pressure region ($P/P_0 > 0.45$), an H3-type hysteresis loop was generated by the capillary condensation. The above results indicated that the Ni/bentonite-U and Ni-2wt%Mn/bentonite-U catalysts both were mesoporous materials with a layered structure [45].

From the pore size distribution curve in Figure 5B, the pore sizes of the two catalysts were in a narrow range between 2 and 20 nm. After adding Mn, the pore size of Ni/bentonite-U catalyst did not significantly change, which indicated that adding Mn exhibited no significant effect on the catalyst pore size distribution.

Table 1. Texture properties of the Ni/Bentonite-U and Ni-2wt%Mn/Bentonite-U catalysts.

Catalysts	S_{BET} [1] $(m^2 \cdot g^{-1})$	Average Pore Diameter (nm)	Pore Volume $(mL \cdot g^{-1})$	Ni Dispersion [2] (%)
Bentonite [3]	75.7	10.6	0.200	-
Ni/bentonite-U[3]	79.8	11.4	0.228	18.9
Ni-2wt%Mn/bentonite-U	92.6	8.8	0.203	22.1

[1] Determined by N_2 adsorption-desorption analysis; [2] Determined by H_2 pulse chemisorption; [3] the data was showed in Reference [25].

In general, the larger the specific surface area of the catalyst, the more active sites can be provided for the reactant molecule, to a certain extent, which is beneficial to improve the catalytic activity of the catalyst [4]. In Table 1, the BET surface area of the Ni-2wt%Mn/Bentonite-U ($92.6 \ m^2 \cdot g^{-1}$) was larger than that of the Ni/bentonite-U ($79.8 \ m^2 \cdot g^{-1}$) and bentonite ($75.7 \ m^2 \cdot g^{-1}$) [26], respectively, and the pore diameter of the Ni-2wt%Mn/bentonite-U (8.8 nm) was also smaller than that of the Ni/Bentonite-U (11.4 nm) and bentonite (10.6 nm), respectively, indicating that the addition of Mn exhibited a reduction of the pore diameter in Ni/bentonite catalysts. The results of Table 1 and XRD data indicated that the addition of Mn promoted the dispersion of NiO species on the surface of bentonite and reduced the blocking of NiO on the carrier pore. It concluded that the addition of Mn had an effect on the pore structure of the catalyst, which made the NiO particles better dispersed in the Ni-Mn/bentonite catalyst, and the catalyst with a larger specific surface area was advantageous to the catalytic activity [46].

In Table 1, the dispersions of metal Ni, determined by H_2 pulse chemisorption, on the Ni/bentonite-U catalyst and Ni-2wt%Mn/bentonite-U catalyst were 18.8% and 22.1%, respectively. It can be seen that the addition of Mn increased the dispersion of the active component Ni in the catalyst, which was consistent with the XRD analysis.

2.6. XPS Analysis

Figure 6 showed the XPS profiles of the Ni 2*p*, O 1*s*, and Mn 2*p* for the Ni/bentonite-U and Ni-2wt%Mn/bentonite-U catalysts, and the surface elemental composition and valence change of the Ni-2wt%Mn/bentonite-U catalyst were studied.

In the Ni 2*p* spectra of Ni/bentonite-U and Ni-2wt%Mn/bentonite-U catalysts, there were five Gaussian fitting peaks. Two peaks in the Ni 2*p* spectra, 873.2 eV and 854.5 eV, were typical binding energies of Ni^{2+}, indicating that Ni existed in the form of Ni^{2+} in the two catalysts [47,48]. The peaks at 879.6 and 861.7 eV were the satellite peaks of the Ni $2p_{1/2}$ and Ni $2p_{3/2}$ [49,50], respectively, and were produced by the orbital spin splitting. In addition, the peak at 856.3 eV and the peak at about 856.2 eV was mainly caused by the presence of nickel-alumina spinel [49,51]. The binding energy of Ni $2p_{3/2}$ belonged to $Ni(OH)_2$ [52], which might be overlapping with the peak of nickel-alumina spinel. With the above analysis and XRD results, the major form for Ni in the catalysts was NiO.

In Table 2, the binding energies of the Ni 2*p* in the Ni-2wt%Mn/bentonite-U catalyst were 0.1–0.3 eV higher than those in the Ni/bentonite-U catalyst, indicating that the addition of Mn acted as an electron promoter which increased the binding energy of Ni in Ni/bentonite-U catalyst and decreased the electron cloud density around Ni. This phenomenon made Ni exist in an electron-deficient state, which would improve catalytic hydrogenation activity. Therefore, the addition of Mn changed the energy state of Ni in the Ni/bentonite-U catalyst, and also the change of binding energy indicated there was an interaction between Ni and Mn [51,53].
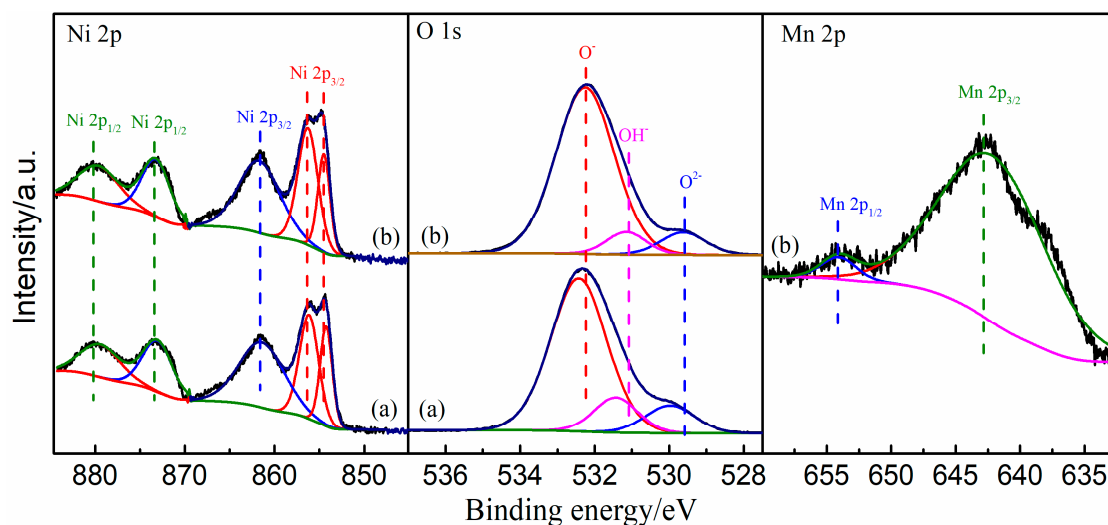
Figure 6. XPS spectra of Ni 2*p*, Mn 2*p*, and O 1*s* regions for Ni/bentonite-U (**a**) and Ni-2wt%Mn/bentonite-U (**b**) catalysts.

Table 2. Binding Energy of Ni 2*p*, Mn 2*p*, and O 1*s* for Ni/bentonite-U and Ni-2wt%Mn/bentonite-U catalysts.

XPS Spectra	Element Valence	Binding Energy (eV) (Percent of Valence State, %)	
		Ni/Bentonite-U	**Ni-2wt%Mn/Bentonite-U**
Ni 2p	$Ni^{2+}(Ni\ 2p_{1/2})$	879.4(14.43)	879.6(14.87)
	$Ni^{2+}(Ni\ 2p_{1/2})$	873.0(16.94)	873.2(16.83)
	$Ni^{2+}(Ni\ 2p_{3/2})$	861.4(32.79)	861.7(31.18)
	$Ni^{2+}(Ni\ 2p_{3/2})$	856.2(22.24)	856.3(24.54)
	$Ni^{2+}(Ni\ 2p_{3/2})$	854.2(13.61)	854.5(12.57)
Mn 2p	$Mn^{4+}(Mn\ 2p_{1/2})$	-	654.0(4.26)
	$Mn^{4+}(Mn\ 2p_{3/2})$	-	642.1(95.74)
O 1s	O^{-}	532.4(74.85)	532.3(83.55)
	OH^{-}	531.4(13.32)	531.2(7.70)
	O^{2-}	529.9(13.32)	529.6.0(8.76)

In the O 1*s* spectra, there were three oxygen species in the two catalysts. The binding energies at 529.9 and 529.6 eV were corresponding to lattice oxygen (O^{2-}). The peaks at 531.4 and 531.2 eV belonged to hydroxyl oxygen (OH^{-}), and the peaks at 532.4 and 532 eV were yielded by surface adsorbed oxygen (O^{-}) [54]. Also, hydroxyl oxygen can be dehydrated to form adsorbed oxygen species under certain conditions [55]. When Mn was added, the binding energies of O 1*s* of the catalysts moved in the direction of low electron binding energies, i.e., towards the characteristic peaks of the lattice oxygen species. In Table 2, the content of surface-adsorbed oxygen in the Ni/bentonite-U catalyst was 83.55% of the total oxygen content, which was 8.7% higher than that of the Ni/bentonite, indicating that the addition of Mn made the catalyst surface produce more surface adsorbed oxygen, representing the amount of oxygen vacancy. The addition of Mn increased the oxygen vacancy in the catalyst which was beneficial to the adsorption and dissociation of CO_2 molecules on the catalyst into intermediate species [54]. In the Mn 2*p* spectrum, the peak located at 642.5 eV corresponded to Mn 2*p* 3/2, and the peak at 653.9 eV was Mn 2*p* 1/2, indicating that the Mn existed as Mn^{4+}, that is, MnO_2 [56,57].

2.7. H_2-TPR Analysis

H_2-TPR was carried out for the Ni/bentonite-U and Ni-2wt%Mn /bentonite-U catalysts, and the effect of Mn addition on the reductive performance of the catalyst and the interaction between metal

and carriers were investigated. The results are shown in Figure 7; each reduction curve was fitted with Gaussian fitting peaks. The calculation results are shown in Table 3.
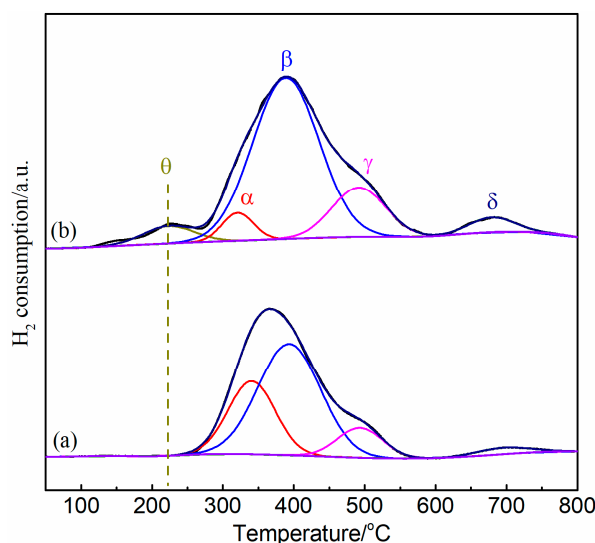

Figure 7. H_2-TPR profiles for Ni/Bentonite-U (a) and Ni-2wt%Mn/Bentonite-U (b) catalysts.

Table 3. Temperatures and area distributions of reduction peaks of Ni/Bentonite-U and Ni-2wt%Mn/Bentonite-U catalysts.

Catalysts	T_{max} Ni Species Reduction (°C)					Peak Area [1] (a.u.)					Total Area (a.u.)
	θ	α	β	γ	δ	θ	α	β	γ	δ	
Ni/bentonite-U	-	340	393	493	696	-	4381	8887	1729	431	15,428
Ni-2wt%Mn/bentonite-U	224	321	389	504	679	1140	1130	13,740	3395	848	20,253

[1] The results were measured from H_2-TPR profiles and the area distributions were calculated by integration of the area under the peaks.

There were four hydrogen reduction peaks (α, β, γ, and δ) in the Ni/bentonite-U and Ni-2wt%Mn/bentonite-U catalysts corresponding to the reduction of NiO species having different interactions with bentonite. The temperature of the reduction peak α in Ni/bentonite-U catalyst (centered at 340 °C) was higher than the temperature of Ni-2wt%Mn/bentonite-U catalyst (321 °C), which corresponded to the reduction of the larger particles of NiO which existed on the surface of the catalyst and had a weak interaction with bentonite [58,59]. The reduction peak β was assigned to the reduction of NiO particles confined within the mesopores, which had a relatively strong interaction with bentonite [58,60]. The peak β temperature did not change significantly in the samples. The reduction peak γ belonged to the reduction of the greater dispersion NiO particles on the surface of bentonite, and the NiO particles had a strong interaction with the support [61]. The temperature of the reduction peak γ (504 °C) in the Ni-Mn/bentonite-U catalyst was higher than that of Ni/bentonite-U catalyst (493 °C). The peak temperature shifted to high temperature, which indicated that the Mn addition enhanced the interaction between support and NiO. The small δ peaks centered at 679 and 696 °C, corresponding to Ni-2wt%Mn/bentonite-U and Ni/bentonite-U catalysts, respectively, were ascribed to the stable nickel aluminate phase with a spinel structure [60,61].

In addition, it is observed that the addition of Mn made the catalyst have a weak reduction peak θ at low temperature (<280 °C), which is attributed to the oxygen species adsorbed on the oxygen vacancy of NiO-Mg oxide solid melt [62], which is consistent with the results of XPS analysis. There were more oxygen vacancies on the surface of the Mn-modified catalyst, but no NiO-Mg oxide solid melt was observed in XRD spectra. The reason might be that the grain size of the material was too small to be detected.

Table 3 showed that the total reduction peak area (20253 a.u.) of Ni-2wt%Mn/bentonite-U catalyst was larger than that of Ni/bentonite-U catalyst (15428 a.u.). The larger the peak area was, the more active the components on the surface of the catalyst were, and the more active sites could be provided, so as to improve the catalytic activity [63]. The reduction peak area proportion of α-type NiO decreased and the β-type NiO proportion increased with the addition of Mn. After the reduction, α-type NiO was the source of large Ni particles, β-type NiO was the source of small Ni particles, and γ-type NiO was the source of fine Ni particles, indicating that the doping of Mn could inhibit the formation of large NiO species in the calcination process of the catalyst [64]. At the same time, the NiO corresponding to the β-reduction peak was also the main Ni source of the catalyst activity at low temperature. The area of the β-reduction peak in Ni-2wt%Mn/bentonite-U catalyst (13740 a.u.) was larger than that of the peak in Ni/bentonite-U catalyst (8887 a.u.). Therefore, Ni-2wt%Mn/bentonite-U catalyst had better catalytic activity at low temperature [65]. This was consistent with the CO_2 methanation activity data in previous Section 2.2.

2.8. Effect of Gas Hourly Space Velocity

Ni-2wt%Mn/bentonite-U catalyst was reduced by H_2 for 2 h under 3600 mL·g_{cat}^{-1}·h^{-1} GHSV. The effects of feed gas GHSV at 2400−8400 mL·g_{cat}^{-1}·h^{-1} on the CO_2 methanation are shown in Figure 8.
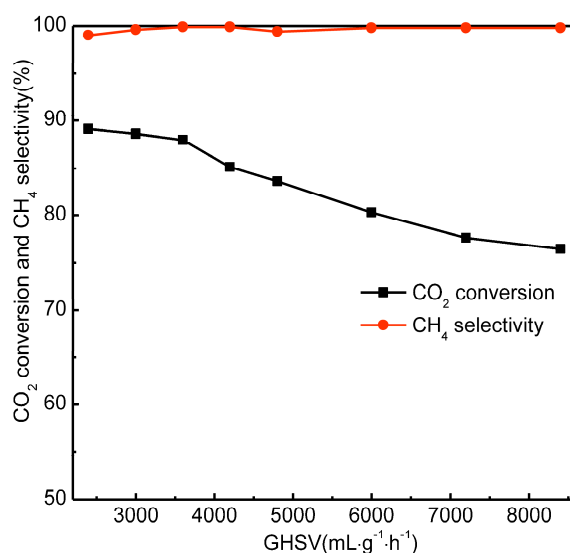

Figure 8. Effect of GHSV on catalytic CO_2 methanation of Ni/bentonite-U and Ni-2wt%Mn/bentonite-U catalysts. Reaction conditions: atmospheric pressure, T = 300 °C, $V(H_2)/V(CO_2)$ = 4.

The CO_2 conversion decreased with the increase of GHSV. When the GHSV increased from 2400 to 8400 mL·g_{cat}^{-1}·h^{-1}, the CO_2 conversion decreased from 89.1% to 76.4%. The reason was that the GHSV increasing reduced the contact time between Ni-2wt%Mn/bentonite-U catalyst and the CO_2/H_2 mixture, causing a lower CO_2 conversion rate. The CO_2 conversion was 88.0% and the selectivity of CH_4 was 100% when the GHSV was 3600 mL·g_{cat}^{-1}·h^{-1}. When the GHSV was higher than 3600 mL·g_{cat}^{-1}·h^{-1}, the CO_2 conversion decreased rapidly. According to the experimental results and the comparability of the data, 3600 mL·g_{cat}^{-1}·h^{-1} was chosen as the optimal GHSV for the investigation of the catalyst stability.

2.9. Stability of Catalysts

The stability of Ni/bentonite and Ni-2wt%Mn/bentonite catalysts was investigated at atmospheric pressure, 300 °C, $V(H_2)/V(CO_2)$ = 4:1, $GHSV$ = 3600 mL·g_{cat}^{-1}·h^{-1}. The results are shown in Figure 9.
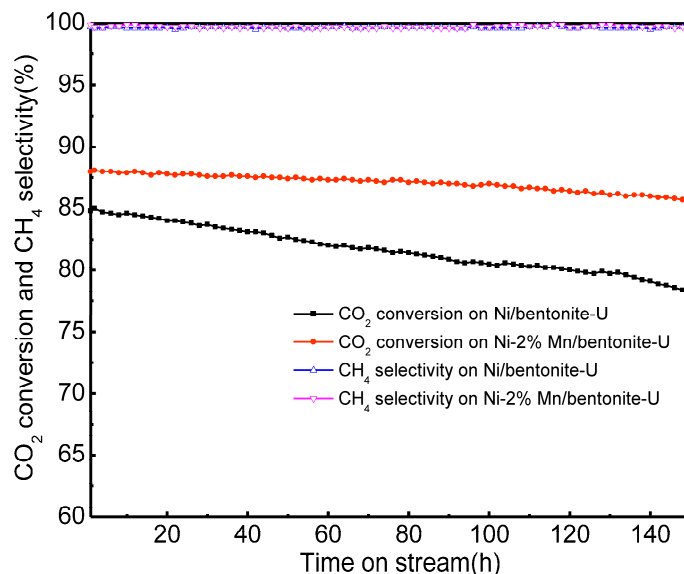
Figure 9. Stability performance of Ni/bentonite and Ni-2wt%Mn/bentonite catalysts. Reaction conditions: atmospheric pressure, T = 300 °C, $V(H_2)/V(CO_2)$ = 4, *GHSV* = 3600 mL·g_{cat}^{-1}·h^{-1}.

During the 150-h reaction, the CO_2 conversion under the catalysis of Ni-2wt%Mn/bentonite catalyst remained at about 87%, and CH_4 selectivity was above 99%. For the Ni/bentonite catalysts, the CO_2 conversion decreased from 84.8% to 78.4%. The results indicated that the Ni-2wt%Mn/bentonite catalysts exhibited a better catalytic stability than the Ni/bentonite catalysts did, and showed a higher catalytic activity at low temperatures.

2.10. Catalyst Characterization after the Reaction

The diffraction peaks of montmorillonite and quartz in the two catalysts after the 150-h stability test are shown in Figure 10. The diffraction peaks of montmorillonite were found at 2θ = 5–10°, which indicated that the layered structure of bentonite was not destroyed after the 150-h reaction. The diffraction peaks at 2θ = 44.6°, 52.0°, and 76.6° (JCPDS card NO.87-0712) corresponded to the crystal plane of Ni (111), (200), and (220). The diffraction peak intensity of Ni in Ni-2wt%Mn/bentonite-U catalyst was weaker than that of Ni in the Ni/bentonite-U catalyst, indicating that Ni particles had good dispersity and stability and a smaller particle size. In addition, the corresponding characteristic diffraction peaks of carbon were not detected in the two catalysts, illustrating the carbon deposition might exist in the amorphous state.

Figure 11 shows the SEM images of Ni-2wt%Mn/bentonite-U and Ni/bentonite-U catalysts after the 150-h reaction. The carbon deposition was not observed on the surface of the two catalysts. In Figure 11A, the Ni particles size was smaller and the particles dispersed uniformly in fresh Ni-2wt%Mn/bentonite-U catalysts. According to Figure 11B, the Ni particles size was obviously aggregated and grew up after the 150-h reaction. However, for the Ni-2wt%Mn/bentonite-U catalysts, the Ni particles were well dispersed and Ni particle size did not show significant change before and after the reaction. With the previous analysis, the Ni particles in the Ni-2wt%Mn/bentonite-U catalysts exhibited a high dispersion with a smaller particle size. The Mn addition enhanced the interaction between NiO and bentonite and inhibited the aggregation and growth of Ni particles during the reaction process (The aggregation and growth of Ni particles would cause the catalytic activity to reduce), which gave the catalyst better stability.
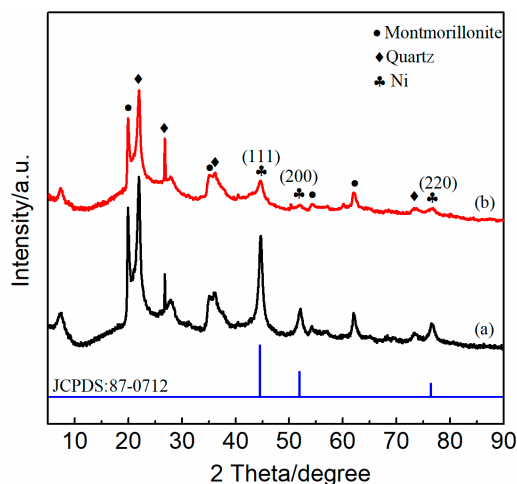
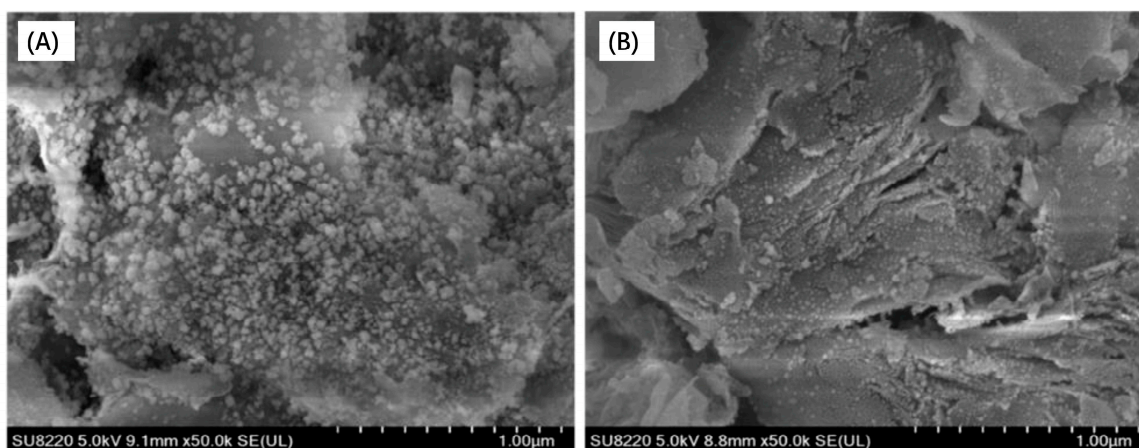**Figure 10.** XRD patterns of Ni/bentonite-U (**a**) Ni-2wt%Mn/bentonite-U (**b**) catalysed after the 150-h reaction.

Figure 11. SEM images of Ni/bentonite-U (**A**), Ni-2wt%Mn/bentonite-U (**B**) catalysed after 150 h stability tests.

3. Experiments

3.1. Catalysts Preparation

The Ni/bentonite catalysts were prepared by using SCS with a 20 wt% metallic Ni loading amount based on the bentonite weight [25]. Typically, to obtain a suspension, 3.0 g bentonite and 2.97 g $Ni(NO_3)_2 \cdot 6H_2O$ were dissolved in 20 mL deionized water, and 3.0 g urea and 0.125, 0.25, and 0.375 mL 50% $Mn(NO_3)_2$ of water solution were added to the above suspension, before being heated to 70 °C and impregnated at 200 r·min^{-1} for 4 h. Subsequently, the above mixture was heated to 400 °C at a 5 °C·min^{-1} heating rate, and kept at 400 °C for 4 h. The obtained catalyst with a Ni loading amount of 20 wt% and a 1.0, 2.0 and 3.0 wt% Mn was marked as Ni-x%Mn/bentonite-U(x = 1.0, 2.0, and 3.0). Accordingly, the Ni-Na/bentonite-U, Ni-Mg/ bentonite-U, Ni-La/ bentonite -U, and Ni-Ce/ bentonite-U catalysts with 2 wt% metal were prepared.

3.2. Catalytic Hydrogenation of CO_2

The catalytic CO_2 methanation on the above Ni-based bentonite catalyst was conducted at atmospheric pressure in a fixed-bed reactor; the detail of the experiments can be found in the literature [25].

3.3. Catalyst Characterization

The XRD, N_2 adsorption-desorption, SEM, XPS, and H_2-TPR were conducted to characterize the catalysts; the details are as described in the literature [25].

4. Conclusions

The Ni/bentonite catalyst was prepared by a solution combustion synthesis and modified by manganese (Mn) as a cocatalyst in the present study. The results showed the Mn modification improved the low-temperature catalytic activity and stability. The Mn-modification Ni/bentonite catalysts exhibited a larger surface area and pore volume, a lower average pore diameter, and a higher metal Ni particles dispersion than the Ni/bentonite catalysts, which would form more Ni activity centers. H_2-TPR analysis showed that the Mn addition increased the total hydrogen consumption of the catalyst and the β-type NiO content, which form the easily reduced Ni species, and led to the Ni-2wt%Mn/bentonite-U catalyst which exhibited better low-temperature activity. XPS results indicated that the Mn addition reduced the electron cloud density around Ni, put the Ni in an electron-deficient state, and more oxygen vacancies were formed on the catalyst surface, which was also beneficial to the CO_2 molecular activation and increased the catalytic activity for CO_2 methanation. Furthermore, Mn addition reduced the Ni particle size and delayed the Ni particles growth in the CO_2 methanation process, which improved the stability of the catalysts. When using Ni-2wt%Mn/bentonite-U as the catalyst, under the condition of atmospheric pressure, 270 °C, $V(H_2)/V(CO_2) = 4$, and a GHSV of 3600 mL·g_{cat}^{-1}·h^{-1}, the CO_2 conversion and CH_4 selectivity were 85.2 and 100%, respectively, which was equivalent to the activities of the Ni/bentonite-U catalyst at 300 °C. In the 150-h stability test, the CO_2 conversion decreased by 2.2% on the Ni-Mn/bentonite catalyst CO_2, while the CO_2 conversion decreased by 6.4% on the Ni/bentonite catalyst.

Author Contributions: Conceptualization, Y.J., Z.Q. and H.J.; investigation, L.D., T.S., and T.H.; writing—original draft preparation, C.X., T.H. and X.X.; writing—review and editing, X.X., B.L., X.L. and Z.Q.

Conflicts of Interest: The authors declare no conflict of interest. The funders had no role in the design of the study; in the collection, analyses, or interpretation of data; in the writing of the manuscript, or in the decision to publish the results.

References

1. Xu, L.; Wang, F.; Chen, M.; Zhang, J.; Yuan, K.; Wang, L.; Wu, K.; Xu, G.; Chen, W. CO_2 methanation over a Ni based ordered mesoporous catalyst for the production of synthetic natural gas. *RSC Adv.* **2016**, *6*, 28489–28499. [CrossRef]

2. IEA. Global Energy & CO_2 Status Report: The Latest Trends in Energy and Emissions in 2017. Available online: https://www.iea.org/publications/freepublications/publication/GECO2017.pdf (accessed on 3 December 2018).

3. Aghaie, M.; Rezaei, N.; Zendehboudi, S. A systematic review on CO_2 capture with ionic liquids: Current status and future prospects. *Renew. Sustain. Energy Rev.* **2018**, *96*, 502–525. [CrossRef]

4. Su, T.; Tian, H.; Qin, Z.; Ji, H. Preparation and characterization of Cu modified $BiYO_3$ for carbon dioxide reduction to formic acid. *Appl. Catal. B* **2017**, *202*, 364–373. [CrossRef]

5. Su, T.; Zhou, X.; Qin, Z.; Ji, H. Intrinsic Kinetics for Dimethyl Ether Synthesis from Plasma Activation CO_2 Hydrogenation over Cu-Fe-Ce/HZSM-5. *ChemPhysChem* **2017**, *18*, 299–309. [CrossRef]

6. Zhou, Y.; Jiang, Y.; Qin, Z.; Xie, Q.; Ji, H. Influence of Zr, Ce, and La on Co_3O_4 catalyst for CO_2 methanation at low temperature. *Chin. J. Chem. Eng.* **2018**, *26*, 768–774. [CrossRef]

7. Wei, W.; Jinlong, G. Methanation of carbon dioxide: An overview. *Front. Chem. Sci. Eng.* **2011**, *5*, 2–10. [CrossRef]

8. Stangeland, K.; Kalai, D.; Li, H.; Yu, Z. CO_2 Methanation: The Effect of Catalysts and Reaction Conditions. *Energy Procedia* **2017**, *105*, 2022–2027. [CrossRef]

9.   Frontera, P.; Macario, A.; Ferraro, M.; Antonucci, P. Supported Catalysts for CO_2 Methanation: A Review. *Catalysts* **2017**, *7*, 59. [CrossRef]

10. Aziz, M.A.A.; Jalil, A.A.; Triwahyono, S.; Ahmad, A. CO_2 methanation over heterogeneous catalysts: Recent progress and future prospects. *Green Chem.* **2015**, *17*, 2647–2663. [CrossRef]

11. Beuls, A.; Swalus, C.; Jacquemin, M.; Heyen, G.; Karelovic, A.; Ruiz, P. Methanation of CO_2: Further insight into the mechanism over $Rh/\gamma\text{-}Al_2O_3$ catalyst. *Appl. Catal. B Environ.* **2012**, *113–114*, 2–10. [CrossRef]

12. Karelovic, A.; Ruiz, P. CO_2 hydrogenation at low temperature over $Rh/\gamma\text{-}Al_2O_3$ catalysts: Effect of the metal particle size on catalytic performances and reaction mechanism. *Appl. Catal. B* **2012**, *113–114*, 237–249. [CrossRef]

13. Garbarino, G.; Riani, P.; Magistri, L.; Busca, G. A study of the methanation of carbon dioxide on Ni/Al_2O_3 catalysts at atmospheric pressure. *Int. J. Hydrogen Energy* **2014**, *39*, 11557–11565. [CrossRef]

14. Yang Lim, J.; McGregor, J.; Sederman, A.J.; Dennis, J.S. Kinetic studies of CO_2 methanation over a $Ni/\gamma\text{-}Al_2O_3$ catalyst using a batch reactor. *Chem. Eng. Sci.* **2016**, *141*, 28–45. [CrossRef]

15. Hu, L.; Urakawa, A. Continuous CO_2 capture and reduction in one process: CO_2 methanation over unpromoted and promoted Ni/ZrO_2. *J. CO_2 Util.* **2018**, *25*, 323–329. [CrossRef]

16. Romero-Sáez, M.; Dongil, A.B.; Benito, N.; Espinoza-González, R.; Escalona, N.; Gracia, F. CO_2 methanation over nickel-ZrO_2 catalyst supported on carbon nanotubes: A comparison between two impregnation strategies. *Appl. Catal. B* **2018**, *237*, 817–825. [CrossRef]

17. Muroyama, H.; Tsuda, Y.; Asakoshi, T.; Masitah, H.; Okanishi, T.; Matsui, T.; Eguchi, K. Carbon dioxide methanation over Ni catalysts supported on various metal oxides. *J. Catal.* **2016**, *343*, 178–184. [CrossRef]

18. Ratchahat, S.; Sudoh, M.; Suzuki, Y.; Kawasaki, W.; Watanabe, R.; Fukuhara, C. Development of a powerful CO_2 methanation process using a structured Ni/CeO_2 catalyst. *J. CO_2 Util.* **2018**, *24*, 210–219. [CrossRef]

19. Yu, Y.; Chan, Y.M.; Bian, Z.; Song, F.; Wang, J.; Zhong, Q.; Kawi, S. Enhanced performance and selectivity of CO_2 methanation over $g\text{-}C_3N_4$ assisted synthesis of $NiCeO_2$ catalyst: Kinetics and DRIFTS studies. *Int. J. Hydrogen Energy* **2018**, *43*, 15191–15204. [CrossRef]

20. Bacariza, M.C.; Bértolo, R.; Graça, I.; Lopes, J.M.; Henriques, C. The effect of the compensating cation on the catalytic performances of Ni/USY zeolites towards CO_2 methanation. *J. CO_2 Util.* **2017**, *21*, 280–291. [CrossRef]

21. Azzolina-Jury, F.; Thibault-Starzyk, F. Mechanism of Low Pressure Plasma-Assisted CO_2 Hydrogenation Over Ni-USY by Microsecond Time-resolved FTIR Spectroscopy. *Top. Catal.* **2017**, *60*, 1709–1721. [CrossRef]

22. Song, H.; Yang, J.; Zhao, J.; Chou, L. Methanation of Carbon Dioxide over a Highly Dispersed Ni/La_2O_3 Catalyst. *Chin. J. Catal.* **2010**, *31*, 21–23. [CrossRef]

23. Ocampo, F.; Louis, B.; Kiwi-Minsker, L.; Roger, A.-C. Effect of Ce/Zr composition and noble metal promotion on nickel based $CexZr_{1-x}O_2$ catalysts for carbon dioxide methanation. *Appl. Catal. A Gen.* **2011**, *392*, 36–44. [CrossRef]

24. Liu, J.; Li, C.; Wang, F.; He, S.; Chen, H.; Zhao, Y.; Wei, M.; Evans, D.G.; Duan, X. Enhanced low-temperature activity of CO_2 methanation over highly-dispersed Ni/TiO_2 catalyst. *Catal. Sci. Technol.* **2013**, *3*, 2627–2633. [CrossRef]

25. Jiang, Y.; Huang, T.; Dong, L.; Qin, Z.; Ji, H. Ni/bentonite catalysts prepared by solution combustion method for low-temperature CO_2 methanation. *Chin. J. Chem. Eng.* **2018**, *26*, 2361–2367. [CrossRef]

26. Zhao, A.; Ying, W.; Zhang, H.; Ma, H.; Fang, D. $Ni\text{-}Al_2O_3$ catalysts prepared by solution combustion method for syngas methanation. *Catal. Commun.* **2012**, *17*, 34–38. [CrossRef]

27. Yi, Y.; Zhang, P.; Qin, Z.; Yu, C.; Li, W.; Qin, Q.; Li, B.; Fan, M.; Liang, X.; Dong, L. Low temperature CO oxidation catalysed by flower-like Ni–Co–O: How physicochemical properties influence catalytic performance. *RSC Adv.* **2018**, *8*, 7110–7122. [CrossRef]

28. Mu, J.; Li, X.; Sun, W.; Fan, S.; Wang, X.; Wang, L.; Qin, M.; Gan, G.; Yin, Z.; Zhang, D. Enhancement of Low-Temperature Catalytic Activity over a Highly Dispersed Fe–Mn/Ti Catalyst for Selective Catalytic Reduction of NO_x with NH_3. *Ind. Eng. Chem. Res.* **2018**, *57*, 10159–10169. [CrossRef]

29. Zhao, A.; Ying, W.; Zhang, H.; Ma, H.; Fang, D. La and Mn Promotion of Ni/Al_2O_3 Catalysts for Syngas Methanation. *Energy Source Part A Recover. Util. Environ. Eff.* **2014**, *36*, 1049–1056. [CrossRef]

30. Song, H.; Hu, F.; Peng, Y.; Li, K.; Bai, S.; Li, J. Non-thermal plasma catalysis for chlorobenzene removal over $CoMn/TiO_2$ and $CeMn/TiO_2$: Synergistic effect of chemical catalysis and dielectric constant. *Chem. Eng. J.* **2018**, *347*, 447–454. [CrossRef]

31. Jiang, Y.; Li, X.; Qin, Z.; Ji, H. Preparation of Ni/bentonite catalyst and its applications in the catalytic hydrogenation of nitrobenzene to aniline. *Chin. J. Chem. Eng.* **2016**, *24*, 1195–1200. [CrossRef]

32. Jiang, Y.; Huang, T.; Xu, Y.; Li, X.; Qin, Z.; Ji, H. Anti-Coke Properties of Acid-Treated Bentonite-Supported Nickel-Boron Catalyst. *Chem. Eng. Technol.* **2018**, *41*, 175–181. [CrossRef]

33. Huang, C.P.; Richardson, J.T. Alkali promotion of nickel catalysts for carbon monoxide methanation. *J. Catal.* **1978**, *51*, 1–8. [CrossRef]

34. Bacariza, M.C.; Graça, I.; Bebiano, S.S.; Lopes, J.M.; Henriques, C. Magnesium as Promoter of CO_2 Methanation on Ni-Based USY Zeolites. *Energy Fuels* **2017**, *31*, 9776–9789. [CrossRef]

35. Wang, F.; He, S.; Chen, H.; Wang, B.; Zheng, L.; Wei, M.; Evans, D.G.; Duan, X. Active Site Dependent Reaction Mechanism over Ru/CeO_2 Catalyst toward CO_2 Methanation. *J. Am. Chem. Soc.* **2016**, *138*, 6298–6305. [CrossRef] [PubMed]

36. Konishcheva, M.V.; Potemkin, D.I.; Snytnikov, P.V.; Stonkus, O.A.; Belyaev, V.D.; Sobyanin, V.A. The insights into chlorine doping effect on performance of ceria supported nickel catalysts for selective CO methanation. *Appl. Catal. B* **2018**, *221*, 413–421. [CrossRef]

37. Mullins, D.R. The surface chemistry of cerium oxide. *Surf. Sci. Rep.* **2015**, *70*, 42–85. [CrossRef]

38. Konishcheva, M.V.; Potemkin, D.I.; Badmaev, S.D.; Snytnikov, P.V.; Paukshtis, E.A.; Sobyanin, V.A.; Parmon, V.N. On the Mechanism of CO and CO_2 Methanation Over Ni/CeO_2 Catalysts. *Top. Catal.* **2016**, *59*, 1424–1430. [CrossRef]

39. Frontera, P.; Macario, A.; Monforte, G.; Bonura, G.; Ferraro, M.; Dispenza, G.; Antonucci, V.; Aricò, A.S.; Antonucci, P.L. The role of Gadolinia Doped Ceria support on the promotion of CO_2 methanation over Ni and NiFe catalysts. *Int. J. Hydrogen Energy* **2017**, *42*, 26828–26842. [CrossRef]

40. Bernal, S.; Blanco, G.; El Amarti, A.; Cifredo, G.; Fitian, L.; Galtayries, A.; Martín, J.; Pintado, J.M. Surface basicity of ceria-supported lanthana. Influence of the calcination temperature. *Surf. Interface Anal.* **2006**, *38*, 229–233. [CrossRef]

41. McFarland, E.W.; Metiu, H. Catalysis by Doped Oxides. *Chem. Rev.* **2013**, *113*, 4391–4427. [CrossRef]

42. Guo, J.; Hou, Z.; Gao, J.; Zheng, X. DRIFTS Study on Adsorption and Activation of CH_4 and CO_2 over Ni/SiO_2 Catalyst with Various Ni Particle Sizes. *Chin. J. Catal.* **2007**, *28*, 22–26. [CrossRef]

43. Zhou, J.; Ma, H.; Jin, F.; Zhang, H.; Ying, W. Mn and Mg dual promoters modified $Ni/\alpha-Al_2O_3$ catalysts for high temperature syngas methanation. *Fuel Process. Technol.* **2018**, *172*, 225–232. [CrossRef]

44. Miao, G.; Zan, Y.; Sun, Y.; Wang, H.; Li, S.; Liu, C.; Li, S.; Kong, L.; Sun, Y. Mn-promoted hydrogenation of microalgae (*Chlorococcum* sp.) to 1,2-propanediol and ethylene glycol over Ni-ZnO catalysts. *Appl. Catal. A* **2018**, *565*, 34–45. [CrossRef]

45. Mendoza de la Cruz, J.L.; Castellanos-Ramírez, I.V.; Ortiz-Tapia, A.; Buenrostro-González, E.; Durán-Valencia, C.D.L.A.; López-Ramírez, S. Study of monolayer to multilayer adsorption of asphaltenes on reservoir rock minerals. *Colloids Surf. Physicochem. Eng. Asp.* **2009**, *340*, 149–154. [CrossRef]

46. Liu, Y.; Zhou, W.; Fan, C.Q.; Yin, R. Electrochemical hydrogenation of coal on Ni-based catalysts. *Fuel* **2014**, *122*, 54–59. [CrossRef]

47. Gao, J.; Jia, C.; Li, J.; Gu, F.; Xu, G.; Zhong, Z.; Su, F. Nickel Catalysts Supported on Barium Hexaaluminate for Enhanced CO Methanation. *Ind. Eng. Chem. Res.* **2012**, *51*, 10345–10353. [CrossRef]

48. Zhang, M.; Mu, S.; Guan, Q.; Li, W.; Du, J. A high anticorrosive chromium-free conversion coating prepared with an alkaline conversion bath on electroless Ni–P coating. *Appl. Surf. Sci.* **2015**, *349*, 108–115. [CrossRef]

49. Kaichev, V.V.; Gladky, A.Y.; Prosvirin, I.P.; Saraev, A.A.; Hävecker, M.; Knop-Gericke, A.; Schlögl, R.; Bukhtiyarov, V.I. In situ XPS study of self-sustained oscillations in catalytic oxidation of propane over nickel. *Surf. Sci.* **2013**, *609*, 113–118. [CrossRef]

50. Gao, J.; Jia, C.; Li, J.; Zhang, M.; Gu, F.; Xu, G.; Zhong, Z.; Su, F. Ni/Al_2O_3 catalysts for CO methanation: Effect of Al_2O_3 supports calcined at different temperatures. *J. Energy Chem.* **2013**, *22*, 919–927. [CrossRef]

51. Qin, Z.; Ren, J.; Miao, M.; Li, Z.; Lin, J.; Xie, K. The catalytic methanation of coke oven gas over $Ni-Ce/Al_2O_3$ catalysts prepared by microwave heating: Effect of amorphous NiO formation. *Appl. Catal. B* **2015**, *164*, 18–30. [CrossRef]

52. Kesavan, J.K.; Luisetto, I.; Tuti, S.; Meneghini, C.; Battocchio, C.; Iucci, G. Ni supported on YSZ: XAS and XPS characterization and catalytic activity for CO_2 methanation. *J. Mater. Sci.* **2017**, *52*, 10331–10340. [CrossRef]

53. Li, Z.; Zhao, T.; Zhang, L. Promotion effect of additive Fe on Al_2O_3 supported Ni catalyst for CO_2 methanation. *Appl. Organomet. Chem.* **2018**, *32*, e4328. [CrossRef]

54. Zhou, G.; Liu, H.; Cui, K.; Jia, A.; Hu, G.; Jiao, Z.; Liu, Y.; Zhang, X. Role of surface Ni and Ce species of Ni/CeO$_2$ catalyst in CO$_2$ methanation. *Appl. Surf. Sci.* **2016**, *383*, 248–252. [CrossRef]

55. Ding, W.; Chen, Y.; Fu, X. Oxidative coupling of methane over Ce^{4+}-doped Ba$_3$WO$_6$ catalysts: Investigation on oxygen species responsible for catalytic performance. *Catal. Lett.* **1994**, *23*, 69–78. [CrossRef]

56. Baran, R.; Valentin, L.; Dzwigaj, S. Incorporation of Mn into the vacant T-atom sites of a BEA zeolite as isolated, mononuclear Mn: FTIR, XPS, EPR and DR UV-Vis studies. *Phys. Chem. Chem. Phys.* **2016**, *18*, 12050–12057. [CrossRef] [PubMed]

57. Ilton, E.S.; Post, J.E.; Heaney, P.J.; Ling, F.T.; Kerisit, S.N. XPS determination of Mn oxidation states in Mn (hydr)oxides. *Appl. Surf. Sci.* **2016**, *366*, 475–485. [CrossRef]

58. Li, D.; Zeng, L.; Li, X.; Wang, X.; Ma, H.; Assabumrungrat, S.; Gong, J. Ceria-promoted Ni/SBA-15 catalysts for ethanol steam reforming with enhanced activity and resistance to deactivation. *Appl. Catal. B* **2015**, *176–177*, 532–541. [CrossRef]

59. Zhang, J.; Xu, H.; Jin, X.; Ge, Q.; Li, W. Characterizations and activities of the nano-sized Ni/Al$_2$O$_3$ and Ni/La–Al$_2$O$_3$ catalysts for NH$_3$ decomposition. *Appl. Catal. A* **2005**, *290*, 87–96. [CrossRef]

60. Lu, X.; Gu, F.; Liu, Q.; Gao, J.; Liu, Y.; Li, H.; Jia, L.; Xu, G.; Zhong, Z.; Su, F. VO$_x$ promoted Ni catalysts supported on the modified bentonite for CO and CO$_2$ methanation. *Fuel Process. Technol.* **2015**, *135*, 34–46. [CrossRef]

61. Mile, B.; Stirling, D.; Zammitt, M.A.; Lovell, A.; Webb, M. TPR studies of the effects of preparation conditions on supported nickel catalysts. *J. Mol. Catal.* **1990**, *62*, 179–198. [CrossRef]

62. Zheng, W.; Zhang, J.; Ge, Q.; Xu, H.; Li, W. Effects of CeO$_2$ addition on Ni/Al$_2$O$_3$ catalysts for the reaction of ammonia decomposition to hydrogen. *Appl. Catal. B* **2008**, *80*, 98–105. [CrossRef]

63. Tao, X.; Bai, M.; Li, X.; Long, H.; Shang, S.; Yin, Y.; Dai, X. CH$_4$–CO$_2$ reforming by plasma—Challenges and opportunities. *Prog. Energy Combust. Sci.* **2011**, *37*, 113–124. [CrossRef]

64. Sehested, J. Sintering of nickel steam-reforming catalysts. *J. Catal.* **2003**, *217*, 417–426. [CrossRef]

65. Zhao, A.; Ying, W.; Zhang, H.; Hongfang, M.; Fang, D. Ni/Al$_2$O$_3$ catalysts for syngas methanation: Effect of Mn promoter. *J. Nat. Gas Chem.* **2012**, *21*, 170–177. [CrossRef]